Neuron

Article

Precise Spatiotemporal Control of Nodal Na^+ Channel Clustering by Bone Morphogenetic Protein-1/Tolloid-like Proteinases

Graphical Abstract

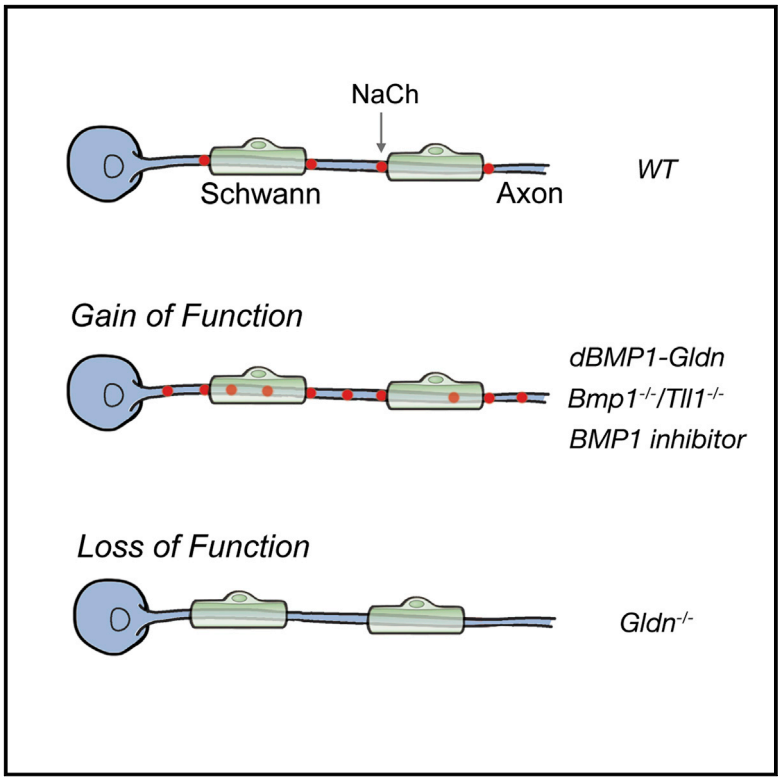

Highlights

- Increased activity of gliomedin causes ectopic and premature Na^+ channel clustering
- The clustering activity of gliomedin is negatively regulated by BMP1/Tolloid-like proteases
- Absence of BMP and *Tll1* results in abnormal clustering of Na^+ channels during myelination

Authors

Yael Eshed-Eisenbach, Jerome Devaux, Anna Vainshtein, ..., Keiichiro Susuki, Matthew N. Rasband, Elior Peles

Correspondence

peles@weizmann.ac.il

In Brief

Eshed-Eisenbach et al. demonstrate that BMP1/Tll1-mediated cleavage of gliomedin provides a regulatory mechanism ensuring that Na^+ channels are clustered at the right time and place during PNS development. By negatively regulating the activity of gliomedin, these enzymes couple between myelination and clustering of Na^+ channels at the nodes of Ranvier.

Eshed-Eisenbach et al., 2020, Neuron *106*, 806–815
June 3, 2020
https://doi.org/10.1016/j.neuron.2020.03.001

CellPress

CellPress

Neuron

Article

Precise Spatiotemporal Control of Nodal Na^+ Channel Clustering by Bone Morphogenetic Protein-1/Tolloid-like Proteinases

Yael Eshed-Eisenbach,[1] Jerome Devaux,[3] Anna Vainshtein,[1] Ofra Golani,[2] Se-Jin Lee,[4] Konstantin Feinberg,[1] Natasha Sukhanov,[1] Daniel S. Greenspan,[5] Keiichiro Susuki,[6] Matthew N. Rasband,[7] and Elior Peles[1,8,*]

[1]Department of Molecular Cell Biology, Weizmann Institute of Science, Rehovot 76100, Israel
[2]Department of Life Sciences Core Facilities, Weizmann Institute of Science, Rehovot 76100, Israel
[3]INSERM U1051, Institut des Neurosciences de Montpellier (INM), Université de Montpellier, 34295 Montpellier, France
[4]The Jackson Laboratory and Department of Genetics and Genome Sciences, University of Connecticut School of Medicine, Farmington, CT 06032, USA
[5]Department of Cell and Regenerative Biology, University of Wisconsin School of Medicine and Public Health, Madison, WI 53705, USA
[6]Department of Neuroscience, Cell Biology, and Physiology, Boonshoft School of Medicine, Wright State University, Dayton, OH 45435, USA
[7]Department of Neuroscience, Baylor College of Medicine, Houston, TX 77030, USA
[8]Lead Contact
*Correspondence: peles@weizmann.ac.il
https://doi.org/10.1016/j.neuron.2020.03.001

SUMMARY

During development of the peripheral nervous system (PNS), Schwann-cell-secreted gliomedin induces the clustering of Na^+ channels at the edges of each myelin segment to form nodes of Ranvier. Here we show that bone morphogenetic protein-1 (BMP1)/Tolloid (TLD)-like proteinases confine Na^+ channel clustering to these sites by negatively regulating the activity of gliomedin. Eliminating the Bmp1/TLD cleavage site in gliomedin or treating myelinating cultures with a Bmp1/TLD inhibitor results in the formation of numerous ectopic Na^+ channel clusters along axons that are devoid of myelin segments. Furthermore, genetic deletion of *Bmp1* and *Tll1* genes in mice using a Schwann-cell-specific Cre causes ectopic clustering of nodal proteins, premature formation of heminodes around early ensheathing Schwann cells, and altered nerve conduction during development. Our results demonstrate that by inactivating gliomedin, Bmp1/TLD functions as an additional regulatory mechanism to ensure the correct spatial and temporal assembly of PNS nodes of Ranvier.

INTRODUCTION

Rapid and efficient saltatory impulse propagation along myelinated axons requires high-density clustering of voltage-gated Na^+ channels at the nodes of Ranvier, which are present between adjacent myelin segments. In peripheral nerves, Na^+ channel clustering is initiated at the edges of the forming myelin segments by binding of gliomedin and NrCAM present on Schwann cell microvilli to axonal neurofascin 186 (NF186) (Feinberg et al., 2010; Labasque et al., 2011). This interaction in turn leads to the clustering of NF186 and further recruitment of the cytoskeletal scaffolding protein Ankyrin G (AnkG) and Na^+ channels (Rasband and Peles, 2015; Zhang et al., 2012). The continuous interaction between gliomedin and NF186 is required not only for the initial clustering of Na^+ channels but also for their long-term maintenance at nodes (Amor et al., 2014; Desmazieres et al., 2014). Human mutations in gliomedin cause lethal congenital contractural syndrome (LCCS; also known as arthrogryposis multiplex congenita), as a result of decreased fetal movement *in utero* (Maluenda et al., 2016; Wambach et al., 2017).

Gliomedin is a transmembrane protein that is shed from Schwann cells by a furin protease, resulting in a secreted form that clusters Na^+ channels on the axolemma (Eshed et al., 2007; Labasque et al., 2011; Maertens et al., 2007). Given the ability of secreted gliomedin to induce clustering of Na^+ channels even in the absence of Schwann cells (Eshed et al., 2005), it is unclear how Na^+ channel clustering is restricted only to the forming nodes of Ranvier. One possibility is that gliomedin is incorporated into the nodal extracellular matrix (ECM) by binding to heparan sulfate proteoglycans, which serves to both localize it and further enhance its clustering activity (Colombelli et al., 2015; Eshed et al., 2007; Maertens et al., 2007). In addition, the activity of gliomedin may be negatively regulated by bone morphogenetic protein-1 (BMP1)/Tolloid (TLD)-like metalloproteinases that cleave the protein in its extracellular domain (ECD; Eshed et al., 2007; Maertens et al., 2007). Such a proteolytic processing separates between the olfactomedin (OLF) domain, which mediates the binding of gliomedin to neurofascin, and the collagen-like (COL) domain, which is required for self-aggregation of gliomedin (Eshed et al., 2007). By using a protease-resistant mutant of gliomedin, pharmacological inhibition of BMP1/TLD enzymes, and genetic deletion of *Bmp1* and the closely homologous Tolloid-like 1 (*Tll1*) gene in Schwann cells, we show that these enzymes negatively regulate the activity of gliomedin during peripheral nervous system (PNS)

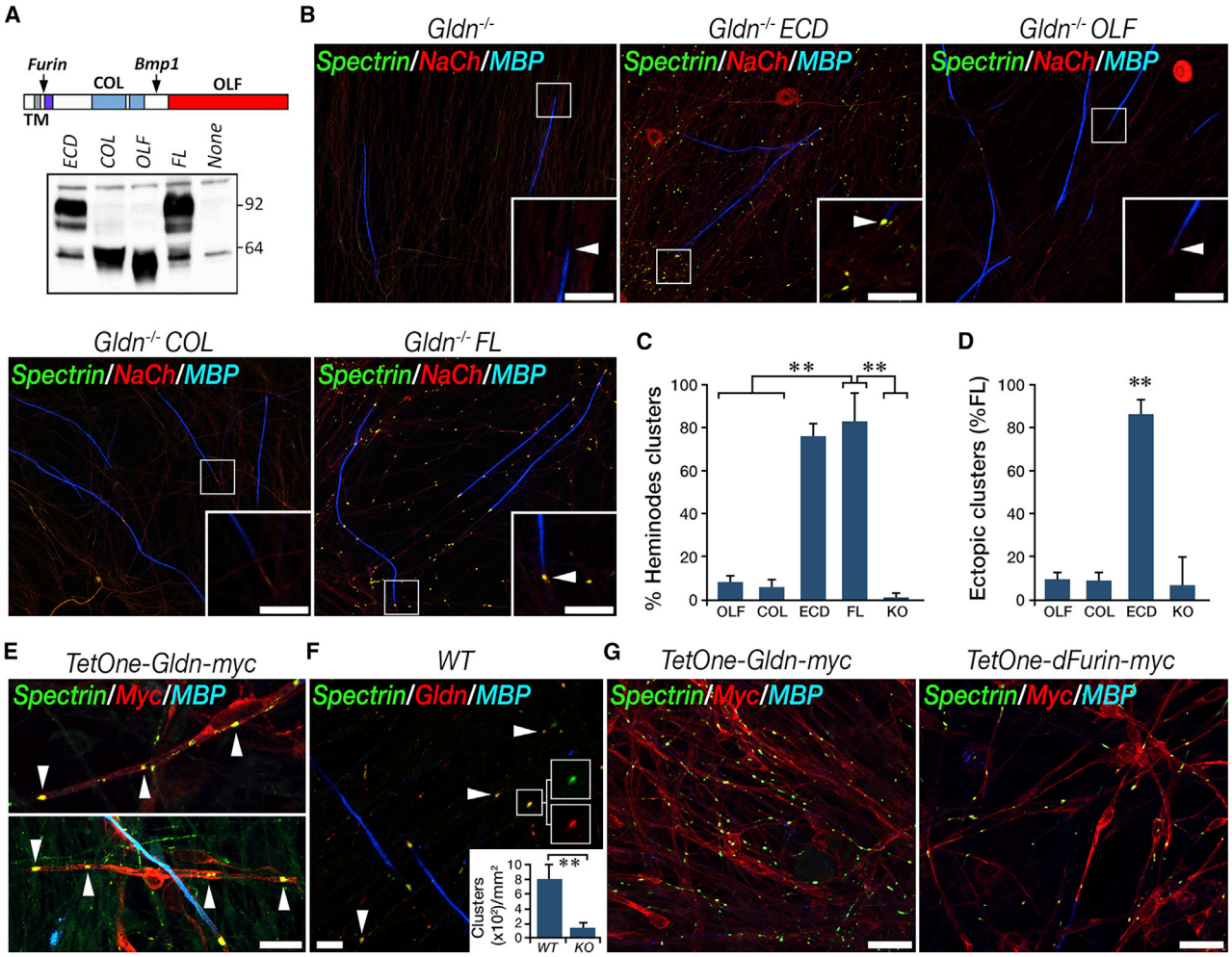

Figure 1. Both the Olfactomedin and Collagen-like Domains of Gliomedin Are Necessary for Glial-Induced Sodium Channel Clustering along DRG Neurons

(A) Schematic representation of the domain organization of gliomedin along with the location of the cleavage sites of furin and BMP1/TLD (arrows) is shown on the top. TM, transmembrane domain; COL, interrupted collagen repeats; OLF, olfactomedin domain. Western blot analysis of HEK293 cells transfected with myc-tagged constructs containing full-length (FL) gliomedin, its extracellular domain (ECD), collagen-like domain (COL), or the olfactomedin domain (OLF). Untransfected cells (None) were used as a control. The locations of molecular weight markers are shown on the right in kilodaltons.

(B) Myelinated Schwann cells/DRG neuron cultures prepared from *gldn*$^{-/-}$ mice were infected with retroviruses carrying the different gliomedin constructs as indicated at the top of each panel. Cultures were immunolabeled using antibodies to βIV spectrin (Spectrin), Na^+ channels (NaCh), and MBP. Clusters containing βIV spectrin and Na^+ channels are detected at both heminodes and along MBP-negative axons (i.e., ectopic sites) only in cultures expressing FL gliomedin or the complete gliomedin ECD.

(C) Percentage of myelinated axonal segments flanked by heminodal clusters of Na^+ channels in cultures expressing the indicated constructs (Bars represent mean + SD;**$p < 0.005$; n = 3 different primary cultures, total of 300 heminodal sites, as determined by MBP staining, were counted for each construct).

(D) Quantification of the percentage of ectopic Na^+ channel clusters in cultures expressing the indicated constructs as a percentage of ectopic clusters induced by FL gliomedin (Bars represent mean + SD;**$p < 0.005$; n = 3 different primary cultures, total of three fields of 3 mm^2 each measured for each construct). The number of clusters in the mutants was normalized to the FL control in order to compare between different experiments that have different baseline clustering and infection levels in one statistical test.

(E) Immunolabeling of myelinated Schwann cell/DRG neuron cultures prepared from *gldn*$^{-/-}$ mice and infected with retroviruses carrying a tetracycline-inducible construct of myc-tagged gliomedin, using antibodies to βIV spectrin (Spectrin), myc-tag (Myc), and MBP. Ectopic clusters (arrowheads) are found along axons that are associated with premyelinated Myc-positive Schwann cells.

(F) Presence of ectopic clusters in wild-type myelinated Schwann cell/DRG neuron cultures. Cultures were labeled using antibodies to βIV spectrin (Spectrin), gliomedin (Gldn), and MBP. Insets show single channels of the cluster present in the boxed area on the right. Note the presence of gliomedin at ectopic clusters. Quantification of the number of ectopic clusters (i.e., not adjacent to a myelin segment) detected in cultures prepared from wild-type (WT) and gliomedin-null (KO) mice is shown on the right. Bars represent mean + SD; **$p < 0.0008$; n = 3 different experiments.

(legend continued on next page)

myelination and thus play a critical regulatory role in the clustering of Na^+ channels along myelinated axons.

RESULTS

Unregulated Activity of Secreted Gliomedin Results in Ectopic Na^+ Channel Clustering

In the absence of gliomedin, Na^+ channels are not clustered at the edges of the forming myelin sheath (i.e., heminodal clustering is abolished; Feinberg et al., 2010; Figures 1B and S1). To examine the function of secreted gliomedin in the assembly of the nodes of Ranvier, we tested whether a soluble protein containing the entire ECD of gliomedin could rescue Na^+ channel clustering in myelinating Schwann cell/dorsal root ganglion (DRG) neuron co-cultures derived from *Gldn*-null mice. Expression in *Gldn*$^{-/-}$ Schwann cells of either a full-length (FL) gliomedin or a secreted version of gliomedin lacking its transmembrane and cytoplasmic regions resulted in the presence of nodal clusters containing Na^+ channels and βIV spectrin at the edges of MBP-labeled internodes (Figures 1A–1C). The ability of soluble gliomedin to rescue nodal clustering was also demonstrated using myelinating cultures from *Gldn*$^{-/-}$ mice that were grown in the presence of a chimeric Fc-fusion protein containing the extracellular region of gliomedin (Figure S1). In contrast, expression of soluble proteins containing either the COL region or the OLF domain alone did not induce nodal clustering. The expression of a FL or a soluble form of gliomedin in Schwann cells not only rescued heminodal clustering but also resulted in the formation of ectopic node-like clusters along axons that were devoid of myelin segments (Figures 1B and 1D). These ectopic clusters were not detected in cultures expressing either the soluble COL or OLF domains, suggesting that the cleavage of gliomedin between these domains by BMP1/TLD negatively regulates its channel clustering activity (Eshed et al., 2007; Maertens et al., 2007; Figure 1A). Immunolabeling of myelinating Schwann cell/DRG neuron co-cultures prepared from *gldn*$^{-/-}$ mice and infected with retroviruses carrying a tetracycline-inducible construct of myc-tagged gliomedin showed that ectopic clusters were located along axons that were associated with premyelinated MBP-negative/Myc-positive Schwann cells (Figure 1E). Myc immunoreactivity was also detected around the Schwann cell, likely due to the binding of gliomedin to heparan sulfate proteoglycans (Eshed et al., 2007). Furthermore, ectopic node-like clusters were also detected in Schwann cell/DRG neuron co-cultures prepared from wild-type mice (Figure 1F). These clusters were associated with gliomedin and were only scarcely detected when the cultures were prepared from *Gldn*$^{-/-}$ mice.

Because shedding of gliomedin from the surface of Schwann cells may involve a proteolytic cleavage by a furin protease (Eshed et al., 2007; Maertens et al., 2007), we examined the formation of the node-like clusters using myelinating Schwann cells expressing a gliomedin mutant in which the furin cleavage site was eliminated (Figures 1G and S2). In marked contrast to cultures expressing the myc-tagged FL gliomedin, cultures expressing a furin-resistant FL form of gliomedin (dfurin-myc) showed only a limited number of ectopic node-like clusters, mostly at sites that were in contact with dfurin-myc-infected Schwann cell processes (Figure 1G). These results show that the ECD of gliomedin secreted by Schwann cells has the ability to induce the clustering of the nodal proteins not only at heminodes but also at ectopic sites along axons that are devoid of myelin segments. Given that during development of the PNS the initial clustering of the nodal proteins is limited to heminodes (Ching et al., 1999; Schafer et al., 2006; Vabnick et al., 1996), these results suggest that the spatial activity of gliomedin must be tightly regulated.

BMP1/TLD Proteases Negatively Regulate the Clustering Activity of Gliomedin

To assess whether the function of gliomedin is negatively regulated by proteolysis, we generated a gliomedin mutant lacking its BMP1/TLD cleavage site (dBMP1; Eshed et al., 2007; Figures S2A–S2D). Similar to the FL protein, when the dBMP1 gliomedin mutant was expressed in Schwann cells, it was found as both a transmembrane protein present at the cell surface and as a secreted protein that was incorporated into the cell-free ECM (Figure S2E). Expression of dBMP1 in *Gldn*$^{-/-}$ Schwann cells co-cultured with DRG neurons resulted in more than a 2-fold increase in the number of ectopic node-like clusters compared with the number of clusters associated with expression of FL wild-type protein (Figures 2A and 2B). Notably, in Schwann cell/DRG neuron co-cultures, cleavage of gliomedin by BMP1/TLD was detected only after the induction of myelination (Figures 2C and 2D). Immunolabeling using antibodies to myelin internodes (MBP) and Na^+ channels antibodies revealed the presence of Na^+ channel clusters at both heminodes and at ectopic sites along the axon (Figure 2E). Both of these cluster types were associated with gliomedin (Figure 2F) and contained all known neuronal nodal components tested (Figures 2E–2G; data not shown for AnkG or NrCAM). We also noted that in some cases, βIV spectrin and neurofascin immunoreactivity was concentrated on one side of the axon perimeter (Figure 2G), reflecting the difference between ectopic clusters that are induced by soluble gliomedin and heminodes, where the entire axonal circumference is contacted by gliomedin-containing Schwann cell microvilli.

As a complementary approach, we examined whether pharmacological inhibition of BMP1/TLD enzymatic activity affects nodal clustering. Immunolabeling of wild-type rat Schwann cell/DRG neuron co-cultures grown in the presence of UK383367, a selective inhibitor of these enzymes (Bailey et al., 2008; Talantikite et al., 2018), with antibodies to nodal (βIV spectrin) and myelin (MBP) proteins revealed a substantial increase in the number of ectopic clusters (Figures 2H and 2I). Co-labeling of UK383367-treated cultures using an antibody

(G) Formation of ectopic clusters requires furin-dependent shedding of gliomedin. Myelinated Schwann cell/DRG neuron cultures from *gldn*$^{-/-}$ mice were infected with retroviruses carrying a tetracycline-inducible construct of myc-tagged FL gliomedin (*TetOne-Gldn-myc*) or a FL gliomedin mutant lacking its furin cleavage site (*TetOne-dFurin-myc*). Cultures were immunolabeled using antibodies to βIV spectrin (Spectrin), myc tag (Myc), and MBP.
Scale bars, 50 μm (B), 10 μm (E and F), and 20 μm (G). See also Figure S1.

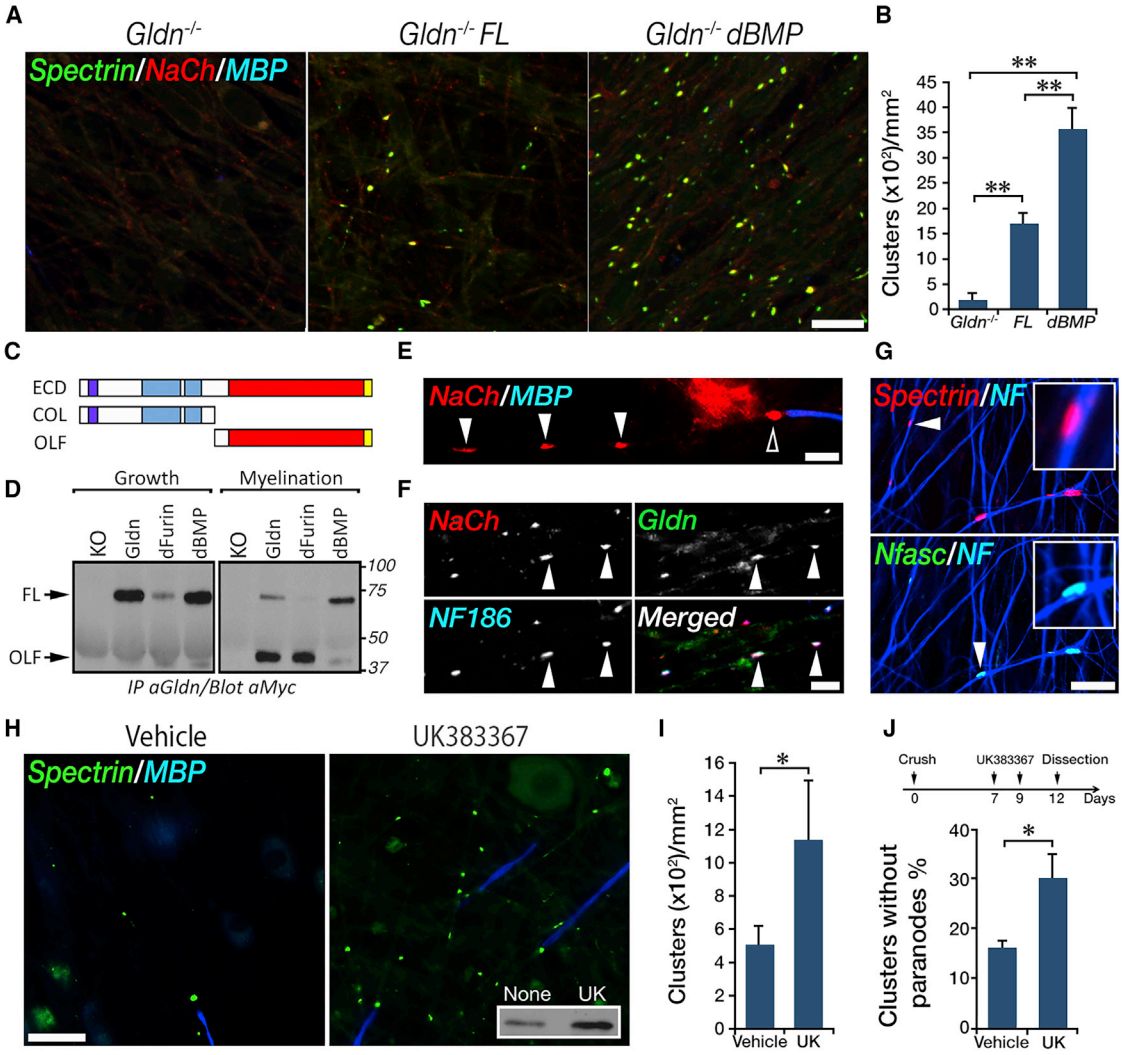

Figure 2. BMP1/TLD-like Proteinases Negatively Regulate the Sodium Channel Clustering Activity of Gliomedin

(A) A BMP1/TLD-resistant mutant of gliomedin enhances the formation of ectopic Na^+ channel clustering. Myelinated Schwann cell/DRG neuron cultures prepared from *Gldn*$^{-/-}$ mice were infected with retroviruses carrying gliomedin (FL) or a gliomedin mutant lacking its BMP1/TLD cleavage site (dBMP). Cultures were immunolabeled using antibodies to βIV spectrin (Spectrin), Na^+ channels (NaCh), and MBP.

(B) Quantification of the results is presented as the number of clusters per square millimeter. Bars represent mean + SD; **$p < 0.005$; n = 3 different experiments representing a total of 15 fields of view counted for each construct.

(C) Schematic presentation of the extracellular domain (ECD) of gliomedin and the two fragments (COL and OLF) obtained after BMP1/TLD-like proteinase cleavage. Yellow square marks the location of the myc tag.

(D) Cleavage of gliomedin by BMP1/TLD proteinases in culture is induced by myelination. Schwann cell/DRG neuron cultures prepared from *Gldn*$^{-/-}$ mice were left untreated (KO) or infected with retroviruses carrying myc-tagged gliomedin (Gldn) or gliomedin mutants lacking either the furin (dFurin) or BMP1/TLD-like (dBMP) proteinase cleavage sites. Cultures were left in either growth or myelination conditions for 7 days, followed by immunoprecipitation and western blot analysis of the medium using antibodies to gliomedin and myc. The location of gliomedin (FL) and the cleaved olfactomedin domain (OLF) are marked on the left and the location of molecular weight markers in kilodaltons on the right.

(E–G) Myelinated *Gldn*$^{-/-}$ cultures infected with a retrovirus that drives the expression of a gliomedin mutant lacking its BMP1/TLD proteinase cleavage site in Schwann cells. Immunolabeling was carried out using antibodies to Na^+ channels (NaCh) and MBP (E), Na^+ channels (NaCh), gliomedin (Gldn) and neurofascin 186 (NF186) (F), and neurofilament (NF) and βIV spectrin (Spectrin) (G, upper panel), or pan-neurofascin (Nfasc) (G, lower panel). (E) Na^+ channel clustering is detected at heminode (open arrowhead) and ectopic sites (arrowheads) along the same axon. (F) Ectopic Na^+ channel clusters contain gliomedin and NF186. (G) Ectopic clusters often do not encompass the entire axon circumference. Insets show higher magnification of the areas marked with arrowheads.

(H) Chemical inhibition of BMP1/TLD proteinases induces the formation of ectopic clusters. Myelinated rat Schwann cell/DRG neuron cultures were either left untreated (None) or treated with BMP1/TLD-like proteinase inhibitor (UK383367) before fixing and labeling using antibodies to βIV spectrin (Spectrin) and MBP. Inset shows western blot analysis of the culture medium using an antibody to gliomedin.

(I) Quantification of the results is presented as the number of ectopic clusters (i.e., not adjacent to a myelin segment) per square millimeter. Bars represent mean + SD; *$p < 0.05$; n = 3 different experiments representing a total of 15 fields of view counted for each condition.

(legend continued on next page)

to myelin-associated glycoprotein (MAG), which marks premyelinating Schwann cells, showed the presence of clusters at heminodes that flanked MAG-positive but MBP-negative internodes, as well as below the forming internode, and at ectopic sites not associated with differentiating Schwann cells (Figure S3A). Most notably, UK383367 did not induce the formation of ectopic clusters in myelinated Schwann cell/DRG neuron co-cultures that were prepared from *gldn*$^{-/-}$ mice (Figure S3B), demonstrating that the induction of such clusters by UK383367 required the expression of gliomedin. Furthermore, we found that the injection of UK383367 into tibial nerves after crush (i.e., during remyelination) resulted in a significant increase in the number of clusters that formed independently from paranodal junctions, as determined by Caspr or pan-neurofascin immunoreactivity (Figure 2J; Figures S3C and S3D). Taken together, these results show that the clustering activity of gliomedin is negatively regulated during myelination by a BMP1/TLD-mediated proteolytic cleavage.

Absence of BMP and Tolloid-like (*Tll1*) Proteases Results in Ectopic Channel Clustering

To further demonstrate that BMP1/TLD-like enzymes play a regulatory role in the assembly of PNS nodes of Ranvier, we examined the expression of *Bmp1* and the related Tll1 gene (Ge and Greenspan, 2006) in peripheral nerve, as well as in isolated Schwann cells and DRG neurons (Figures 3A and 3B). We detected the expression of transcripts from both genes in sciatic nerves and Schwann cells, but not (or only faintly) in isolated DRG neurons. Developmental analysis of sciatic nerve revealed a clear increase in the expression of Tll during early myelination and the time when node assembly is completed, whereas the level of Bmp1 did not seem to change (Figure S4A). We generated mice lacking both *Bmp1* and *Tll1* genes in Schwann cells by crossing mice with floxed alleles of both *Bmp1* and *Tll1* (*Bmp1*$^{fl/fl}$/*Tll*$^{fl/fl}$) (Muir et al., 2014) with Desert Hedgehog (DHH)-Cre transgenic mice (DHH-Cre), in which Cre is active in Schwann cell precursors from embryonic day (E) 12.5 (Jaegle et al., 2003). The resulting *DHH-Cre;Bmp1*$^{fl/fl}$/*Tll*$^{fl/fl}$ mice were viable, showed no overt neurological abnormalities, and exhibited peripheral myelin that was indistinguishable from their wild-type counterparts (Figures S4B–S4H). Myelinating Schwann cell/DRG neuron co-cultures prepared from *DHH-Cre;Bmp1*$^{fl/fl}$/*Tll*$^{fl/fl}$ and control *Bmp1*$^{fl/fl}$/*Tll*$^{fl/fl}$ mice showed that the deletion of *Bmp1* and *Tll1* caused a significant increase in the number of ectopic clusters (Figures 3C and 3D). As expected, the observed ectopic clusters were invariably associated with gliomedin (Figure 3E). Co-labeling with antibodies to MAG and MBP demonstrated the presence of ectopic node-like clusters beneath MAG-positive ensheathing Schwann cells that did not express MBP (Figure 3F). Although most of these internodal clusters were not found in mature MBP-positive segments, infrequently we detected a persistent node-like cluster that was present in the middle of a myelinated internode (Figure 3G, open arrowhead).

Mice Lacking *Bmp1* and *Tll1* in Schwann Cells Display Abnormal Sodium Channel Clustering

We next examined the distribution of βIV spectrin in developing sciatic nerves during the time they undergo myelination in the PNS. Using either whole-mount preparations or frozen sections of sciatic nerves of 3-day-old mice (a time at which we detected a decreased cleavage of gliomedin in *DHH-Cre;Bmp1*$^{fl/fl}$/*Tll*$^{fl/fl}$ mutant; Figures S4I and S4J), we detected a clear and significant increase in the number of βIV spectrin clusters in *DHH-Cre;Bmp1*$^{fl/fl}$/*Tll*$^{fl/fl}$ compared with *Bmp1*$^{fl/fl}$/*Tll*$^{fl/fl}$ control samples (Figures 4A and 4B). We also noted a similar difference between these genotypes using antibodies to gliomedin (Figure 4B), Na^+ channels, or neurofascin (Figure 4F and data not shown). The relative increase in numbers of clusters in *DHH-Cre;Bmp1*$^{fl/fl}$/*Tll*$^{fl/fl}$ samples was observed in peroneal nerves from newborns to postnatal day (P) 5 (Figure 4C), a developmental interval that encompasses the active period of node formation in peripheral nerves (Ching et al., 1999; Schafer et al., 2006; Vabnick et al., 1996). Immunolabeling of teased peroneal nerves using antibodies to Na^+ channels and Caspr revealed a significant increase in the number of clusters that were not associated with Caspr-labeled paranodal junctions at P1 and P3 (Figure 4D), hence corresponding to either early premature heminodal or ectopic sites of channel clustering. In contrast to P3, all nodal clusters were flanked by Caspr in adult nerves (Figure 4E). Notably, clusters that were not adjacent to Caspr were not detected in 3-day-old mice lacking gliomedin (Figure 4F), further indicating that the effect *Bmp1* and *Tll1* have on Na^+ channel clustering is via their action on gliomedin.

In order to determine the impact of premature node-like clusters on conduction, we recorded sciatic nerve activity at different postnatal ages from P2 to P50. As early as P2–P3, the CAPs from control littermates showed two distinct components, reflecting the presence of two axonal populations (Figure 4G): a population of unmyelinated axons that conduct action potentials around 0.5 $m \cdot s^{-1}$ and a second faster population conducting action potentials around 1.4 $m \cdot s^{-1}$ at P2 and 2.1 $m \cdot s^{-1}$ at P3. This latter population showed a homogeneous Gaussian distribution at both ages and likely corresponds to axons with active myelination. By P5, the CAPs showed a predominant fast peak with a conduction velocity of 5.4 $m \cdot s^{-1}$. The velocity of the myelinated axon population then progressively increased to 43 $m \cdot s^{-1}$ at P50. Although there were no differences in characteristics of the CAPs between *DHH-Cre;Bmp1*$^{fl/fl}$/*Tll*$^{fl/fl}$ mice and their control *Bmp1*$^{fl/fl}$/*Tll*$^{fl/fl}$ littermates at adult ages (P50), they showed clear differences at earlier stages. At P2 when the premature node-like clusters appear in *DHH-Cre;Bmp1*$^{fl/fl}$/*Tll*$^{fl/fl}$ axons, we found that the first peak of their CAPs did not follow a

(J) Injection of UK383367 into sciatic nerve after crush increased the number of Na^+ channel clusters. Schematic presentation of the experimental outline is shown on the top. Sciatic nerve sections at 12 days after crush from vehicle (None) or UK383367 (UK) injected nerves were immunolabeled with antibodies to βIV spectrin, Na^+ channels, and Caspr, and the percentage of Na^+ channel clusters without adjacent Caspr-labeled paranodes was calculated. Bars represent mean + SEM; *$p < 0.05$; n = 10 animals for experimental group, 100 nodal clusters for each animal.
Scale bars, 10 μm (A and E–G) and 20 μm (H). See also Figures S2 and S3.

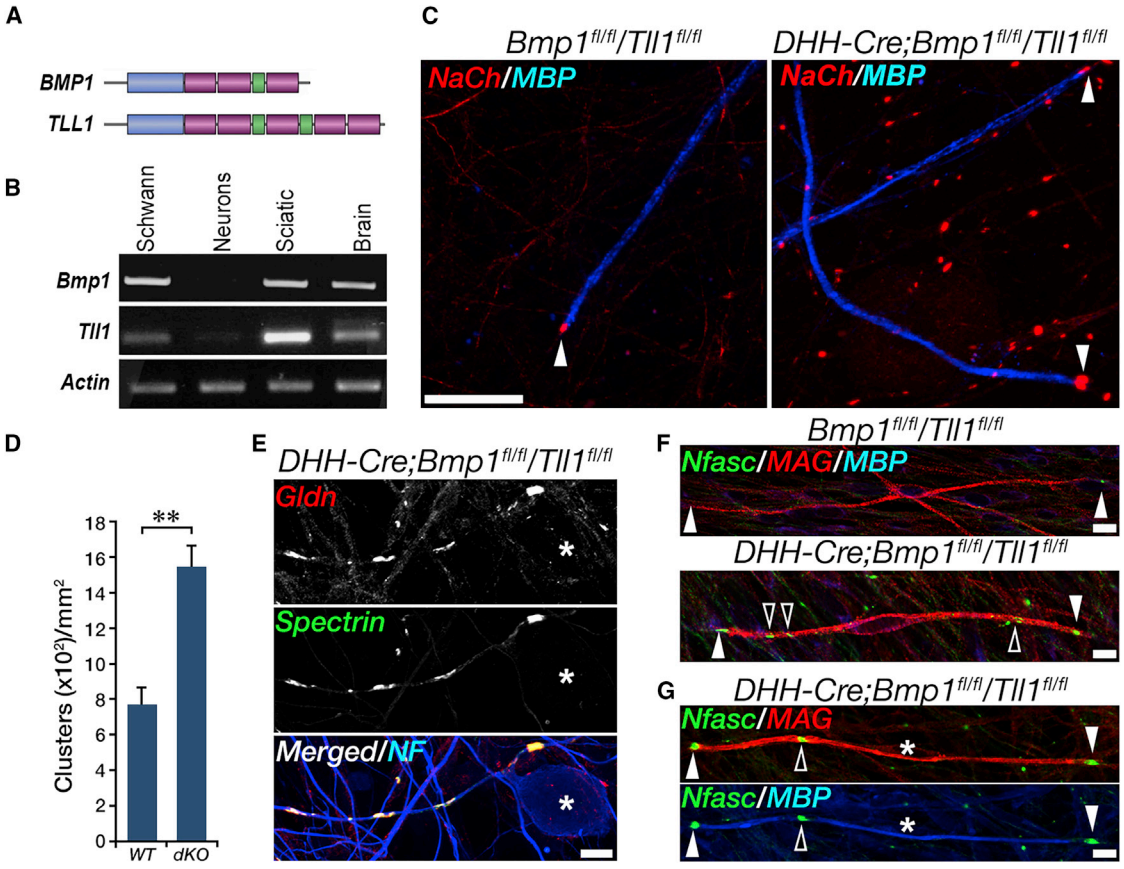

Figure 3. Ablation of Both *Bmp1* and *Tll1* in Schwann Cells Enhances the Formation of Ectopic Na^+ Channel Clustering in Myelinating Cultures

(A) Schematic representation of the domain organizations of bone morphogenetic protein 1 (BMP1) and Tolloid-like 1 (TLL1). BMP1 and a longer proteinase, mammalian Tolloid (mTLD), which has a domain structure (not shown) identical to that of TLL1, are the alternatively spliced products of a single gene (*Bmp1*), whereas TLL1 is encoded by a separate *Tll1* gene.

(B) RT-PCR analysis of mRNA isolated from brain, sciatic nerve, culture Schwann cells, and DRG neurons using primers for *Bmp1*, *Tll1*, and *actin*.

(C) Myelinated Schwann cell/DRG neuron cultures prepared from control mice carrying floxed alleles of both *Bmp1* and *Tll1* ($Bmp1^{fl/fl}/Tll^{fl/fl}$) or animals in which these genes were deleted in Schwann cells using DHH-Cre ($DHH\text{-}Cre;Bmp1^{fl/fl}/Tll^{fl/fl}$) were labeled using antibodies to Na^+ channels (NaCh) and MBP. Arrowheads mark heminodal clusters.

(D) Quantification of the results is presented as the number of ectopic clusters per field of view (FOV). Bars represent mean + SD; $^{**}p < 0.005$; n = 3 different experiments representing a total of 30 fields of view counted for each genotype.

(E) Ectopic clusters induced by deletion of *Bmp1* and *Tll1* are invariably associated with gliomedin. Myelinated $DHH\text{-}Cre;Bmp1^{fl/fl}/Tll^{fl/fl}$ cultures immunolabeled using antibodies to gliomedin (*Gldn*), βIV spectrin (Spectrin), and neurofilament (NF). Asterisk marks the position of a neuronal cell soma.

(F) Ectopic clusters are found in association with early differentiating Schwann cells. Immunolabeling of control ($Bmp1^{fl/fl}/Tll^{fl/fl}$) and double-knockout ($DHH\text{-}Cre;Bmp1^{fl/fl}/Tll^{fl/fl}$) cultures using antibodies to neurofascin (*Nfasc*), MAG, and MBP reveals the formation of ectopic clusters in areas that are located beneath MAG-positive ensheathing Schwann cells that do not express MBP. Arrowheads and open arrowheads mark heminodal and ectopic clusters, respectively.

(G) Presence of a persistent ectopic cluster (open arrowhead) within a single myelinated internode that is flanked by two heminodes (arrowheads). An asterisk marks the location of the Schwann cell nucleus.

Scale bars, 20 μm (C) and 10 μm (E–G).

Gaussian distribution but was multiphasic. The conduction velocity at maximal peak amplitude appeared faster in $DHH\text{-}Cre;Bmp1^{fl/fl}/Tll^{fl/fl}$ animals, but this was not significant, as the potentials were multiphasic. In order to quantify this effect, we measured the delay of the first detectable CAP peak (Figure 4G, arrows). We found that the $DHH\text{-}Cre;Bmp1^{fl/fl}/Tll^{fl/fl}$ mice present an axonal population that conducts faster (2.5 $m \cdot s^{-1}$) than most axons from control animals (Table S1). Similarly, at P3, the CAPs from these animals were multiphasic and presented axonal populations that conducted at higher velocities than normal animals (Figure 4; Table S1). With the reduction in abnormal clustering of nodal proteins at P5 (Figures 4C and 4D), the differences between the CAPs of the different genotypes disappeared, and both strains presented similar conduction velocities. We did not find any differences in the recruitment or refractory period at any ages. Altogether, these data indicate that the premature clustering of Na^+ channels increases conduction velocity

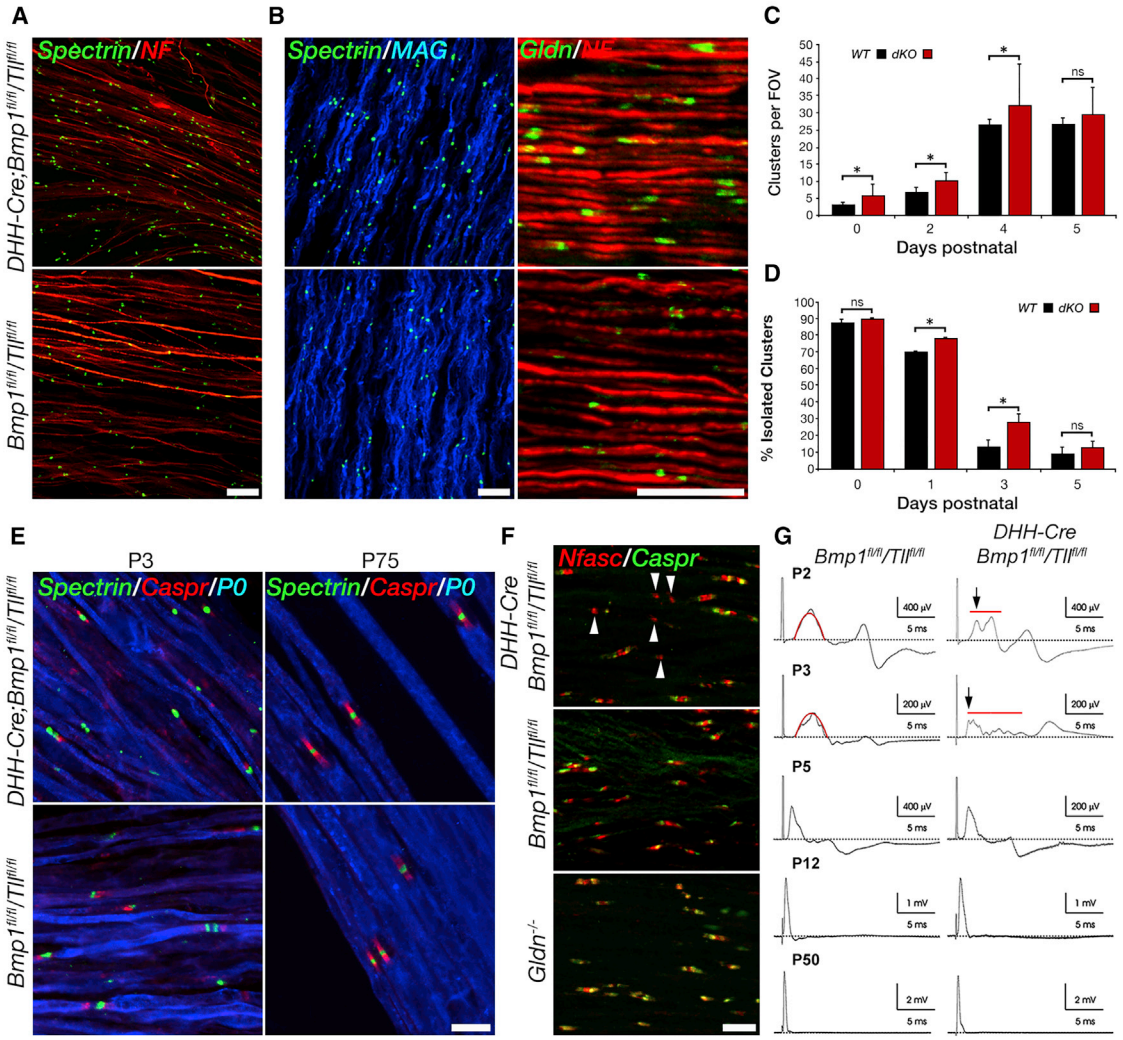

Figure 4. Genetic Deletion of *Bmp1* and *Tll1* in Mice Causes Ectopic Clustering of Sodium Channels and Altered Nerve Conduction during Developmental Myelination

(A and B) Confocal images of whole-mount (A) and longitudinal sciatic nerve sections (B) of P3 control (*Bmp1*$^{fl/fl}$/*Tll*$^{fl/fl}$) and Schwann-specific double-knockout (*DHH-Cre;Bmp1*$^{fl/fl}$/*Tll*$^{fl/fl}$) mice immunolabeled using antibodies to βIV spectrin (Spectrin), neurofilament (NF), MAG, and gliomedin (Gldn) as indicated.

(C) Quantification of the number of βIV spectrin clusters per field of view (FOV) as normalized by DAPI labeling, detected in sciatic nerves of wild-type (WT) and double-knockout (dKO) mice at the indicated postnatal days.

(D) Percentage of clusters that are not associated with Caspr-labeled paranodes in peroneal nerve of wild-type (WT) and the double-knockout (dKO) mice at the indicated postnatal days. Bars represent mean + SD; *$p < 0.05$; $n = 3$ mice for each genotype, representing a total of nine fields of view counted for each genotype at each age. ns, not significant.

(E) Confocal images of sciatic nerves isolated from P3 (left) and P75 (right) mice of the indicated genotypes immunolabeled with antibodies to βIV spectrin (Spectrin), Caspr, and P0. In adult nerves all clusters were confined to the nodes of Ranvier.

(F) Confocal images of P3 peroneal nerve of the indicated genotypes immunolabeled with antibodies to neurofascin (Nfasc) and Caspr. Note the complete absence of clusters lacking adjacent Caspr labeling in *Gldn*-null mice.

(G) Premature Na^+ channel clustering enhances conduction velocity. Sciatic nerves from *DHH-Cre;Bmp1*$^{fl/fl}$/*Tll*$^{fl/fl}$ mice and their control littermates were recorded at P2, P3, P5, P12, and P50 as indicated. At P2 and P3, control CAPs showed two phases: a slow conducting phase reflecting unmyelinated axons and a fast conducting potential reflecting the axon population ongoing myelination. This latter could be fitted with a Gaussian function (red curved line in control *Bmp1*$^{fl/fl}$/*Tll*$^{fl/fl}$ mice). As myelination proceeded, the conduction velocity progressively increased from P5 to P50. No differences were observed at P5, P12, and P50 between the two genotypes. However, at both P2 and P3, the CAPs from *DHH-Cre;Bmp1*$^{fl/fl}$/*Tll*$^{fl/fl}$ mice were multiphasic (red lines) and could not be fitted by a Gaussian function. Note that at these ages, an axonal population conducted faster in the double-mutant mice (arrows) than in control littermates.

Scale bars, 20 μm (A and B) and 10 μm (E and F). See also Figures S3 and S4.

along developing myelinating axons and variability in conduction between different axons.

DISCUSSION

Clustering of Na^+ channels at the nodes of Ranvier is a prerequisite for fast and accurate propagation of action potentials along myelinated axons. In the PNS, assembly of the nodes of Ranvier is initiated by myelinating Schwann cells through the binding of gliomedin to axonal NF186 (Eshed et al., 2005; Feinberg et al., 2010) and its clustering and stabilization on the surface of the axolemma (Zhang et al., 2012). Our present results reveal an important role for BMP1/TLD-like proteinases in confining Na^+ channel clusters to the developing nodes of Ranvier by negatively regulating the activity of gliomedin. This conclusion is based on the following findings: (1) expression of gliomedin's extracellular region, but not its OLF or COL domains, in Schwann cells grown with DRG neurons induced numerous ectopic Na^+ channel clusters along axons that were devoid of myelin segments; (2) eliminating the BMP1/TLD cleavage site in gliomedin induced the formation of ectopic axonal Na^+ channel clusters; (3) a similar increase in the formation of ectopic clusters was observed in mixed Schwann cell/DRG neurons co-cultures grown in the presence of a BMP1/TLD inhibitor; (4) pharmacological induction of ectopic clusters by a BMP1/TLD inhibitor was not detected using Schwann cell/DRG neurons isolated from *Gldn*-null mice; and (5) genetic deletion of *Bmp1* and *Tll1* genes in Schwann cells caused ectopic Na^+ channel clustering, as well as premature formation of heminodes around early ensheathing premyelinating Schwann cells. We have previously shown that gliomedin is enriched at Schwann cell microvilli that appose the axolemma already at an early phase of PNS myelination (Eshed et al., 2005). We propose that upon secretion, gliomedin binds its axonal receptor, NF186, at heminodes, leading to the clustering of Na^+ channels, while the remaining protein molecules are subjected to cleavage by BMP1 and Tll1. This process likely generates low levels of active gliomedin away from the Schwann cell microvilli, thus preventing clustering at ectopic sites. Our results reveal that both the secretion of gliomedin, which potentiates its Na^+ channel clustering activity, and its inactivation are controlled by two distinct proteolytic systems.

The clustering of Na^+ channels along myelinated axons is achieved through the action of distinct adhesion molecules that mediate axon-glia contact at the node of Ranvier and the paranodal junction (Eshed-Eisenbach and Peles, 2013; Rasband and Peles, 2015). The cleavage of gliomedin by BMP1/TLD provides an additional regulatory mechanism that ensures that Na^+ channels are clustered at the right time (i.e., with the appearance of MBP-positive myelin segments) and place (i.e., at heminodes located at the edges of the myelin segments) during development of peripheral nerves. In the absence of this mechanism, Na^+ channels cluster prematurely, resulting in wider range of axonal conduction velocities that could affect the development of central circuits. The absence of BMP1/TLD also leads to earlier heminodal clustering of Na^+ channels around immature MBP-negative internodes. During normal development, gliomedin accumulates at the edges of new MBP-containing segments, where it clusters nodal components right before the paranodal junction forms and seals the structure for efficient saltatory conduction. Thus, by controlling the availability of gliomedin, BMP1/TLD provides spatiotemporal regulation on sodium channel clustering during peripheral nerve development and essentially couples between myelination and the formation of the node of Ranvier. Interestingly, we did not detect ectopic clusters on Remak fibers. We reason that in order for clusters to form on C-fibers (i.e., away from myelinating Schwann cells) a major buildup in the concentration of gliomedin must occur. Because Bmp1 and Tll1 are secreted from cells other than DHH-expressing Schwann cells, such a buildup is probably prevented. BMP1/TLD proteinases couple and orchestrate myelination and node formation, thereby allowing synchronized transition from continuous to saltatory conduction. The regulation of Na^+ channel clustering at heminodes by gliomedin during developmental myelination is likely more functionally significant in humans compared with mice, because humans have much longer axons, and their myelination occurs over several months (Ching et al., 1999; Schafer et al., 2006; Vabnick et al., 1996). In line with this idea, whereas $Gldn^{-/-}$ mice exhibit no clear neurologic deficits or altered nerve conduction in peripheral nerves (Feinberg et al., 2010), loss-of-function mutations in gliomedin in humans causes LCCS associated with decreased fetal movement *in utero*, likely due to abnormal nerve conduction (Maluenda et al., 2016; Wambach et al., 2017).

Although excess amounts of gliomedin in *DHH-Cre;Bmp1*$^{fl/fl}$/*Tll*$^{fl/fl}$ mice induced the formation of ectopic Na^+ channel clusters on axons and under the membranes of premyelinating Schwann cells (i.e., MBP negative), these clusters were transient and were cleared from the internodes with the completion of myelination. In line with this observation, adult *DHH-Cre;Bmp1*$^{fl/fl}$/*Tll*$^{fl/fl}$ mice did not display behavioral abnormalities. As suggested previously (Dzhashiashvili et al., 2007), such a clearance mechanism provides yet another level of regulation to ensure the correct clustering of Na^+ channels at the nodes of Ranvier. The conspicuous appearance of ectopic clusters observed in *DHH-Cre;Bmp1*$^{fl/fl}$/*Tll*$^{fl/fl}$ axons in the present study presents a unique model that may assist in resolving the underlying mechanism by which nodal proteins are actively cleared from the internode.

STAR★METHODS

Detailed methods are provided in the online version of this paper and include the following:

- KEY RESOURCES TABLE
- LEAD CONTACT AND MATERIALS AVAILABILITY
- EXPERIMENTAL MODEL AND SUBJECT DETAILS
  - Mouse Models
  - Primary Cultures
- METHOD DETAILS
  - Generation of gliomedin expression and viral plasmids
  - Production of retroviruses
  - Fc-fusion protein production and purification
  - Reverse transcription PCR

- Immunofluorescent labeling
- Immunoprecipitation and immunoblot analysis
- Electrophysiology
- Sciatic nerve crush
- Image Processing and Analysis
- Electron Microscopy

- QUANTIFICATION AND STATISTICAL ANALYSIS
- DATA AND CODE AVAILABILITY

SUPPLEMENTAL INFORMATION

Supplemental Information can be found online at https://doi.org/10.1016/j.neuron.2020.03.001.

ACKNOWLEDGMENTS

We would like to thank Michael Tsoory for his expert advice and support. This work was supported by research grants from the Israel Science Foundation, the Binational Science Foundation, the Dr. Miriam and Sheldon G. Adelson Medical Research Foundation, the National American Brain Foundation, the Lilly Fulop Fund for Multiple Sclerosis Research, the Estate of David Georges Eskinazi, Dahlia and Philip Lawee, Gary Clayman, Ellie Adiel, Agence Nationale de la Recherche (ACAMIN; E.P. and J.D.) under the frame of E-Rare-2, the ERA-Net for Research on Rare Diseases, and from Association Française contre les Myopathies (grant 21532 to J.D.). E.P. is the incumbent of the Hanna Hertz Professorial Chair for Multiple Sclerosis and Neuroscience.

AUTHOR CONTRIBUTIONS

Conceptualization and Writing, Y.E.-E. and E.P.; Methodology, Investigation, and Analysis, Y.E.-E., K.F., A.V., N.S., K.S., and J.D.; Resources, O.G., S.J.-L., M.N.R., and D.S.G.; Supervision, E.P.

DECLARATION OF INTERESTS

The authors declare no competing interests.

Received: August 14, 2019
Revised: January 30, 2020
Accepted: March 2, 2020
Published: March 24, 2020

REFERENCES

Amor, V., Feinberg, K., Eshed-Eisenbach, Y., Vainshtein, A., Frechter, S., Grumet, M., Rosenbluth, J., and Peles, E. (2014). Long-term maintenance of Na+ channels at nodes of Ranvier depends on glial contact mediated by gliomedin and NrCAM. J. Neurosci. *34*, 5089–5098.

Bailey, S., Fish, P.V., Billotte, S., Bordner, J., Greiling, D., James, K., McElroy, A., Mills, J.E., Reed, C., and Webster, R. (2008). Succinyl hydroxamates as potent and selective non-peptidic inhibitors of procollagen C-proteinase: design, synthesis, and evaluation as topically applied, dermal anti-scarring agents. Bioorg. Med. Chem. Lett. *18*, 6562–6567.

Bankhead, P., Loughrey, M.B., Fernández, J.A., Dombrowski, Y., McArt, D.G., Dunne, P.D., McQuaid, S., Gray, R.T., Murray, L.J., Coleman, H.G., et al. (2017). QuPath: open source software for digital pathology image analysis. Sci. Rep. *7*, 16878.

Berg, S., Kutra, D., Kroeger, T., Straehle, C.N., Kausler, B.X., Haubold, C., Schiegg, M., Ales, J., Beier, T., Rudy, M., et al. (2019). ilastik: interactive machine learning for (bio)image analysis. Nat. Methods *16*, 1226–1232.

Ching, W., Zanazzi, G., Levinson, S.R., and Salzer, J.L. (1999). Clustering of neuronal sodium channels requires contact with myelinating Schwann cells. J. Neurocytol. *28*, 295–301.

Colombelli, C., Palmisano, M., Eshed-Eisenbach, Y., Zambroni, D., Pavoni, E., Ferri, C., Saccucci, S., Nicole, S., Soininen, R., McKee, K.K., et al. (2015). Perlecan is recruited by dystroglycan to nodes of Ranvier and binds the clustering molecule gliomedin. J. Cell Biol. *208*, 313–329.

Desmazieres, A., Zonta, B., Zhang, A., Wu, L.M., Sherman, D.L., and Brophy, P.J. (2014). Differential stability of PNS and CNS nodal complexes when neuronal neurofascin is lost. J. Neurosci. *34*, 5083–5088.

Dzhashiashvili, Y., Zhang, Y., Galinska, J., Lam, I., Grumet, M., and Salzer, J.L. (2007). Nodes of Ranvier and axon initial segments are Ankyrin G-dependent domains that assemble by distinct mechanisms. J. Cell Biol. *177*, 857–870.

Eshed, Y., Feinberg, K., Poliak, S., Sabanay, H., Sarig-Nadir, O., Spiegel, I., Bermingham, J.R., Jr., and Peles, E. (2005). Gliomedin mediates Schwann cell-axon interaction and the molecular assembly of the nodes of Ranvier. Neuron *47*, 215–229.

Eshed, Y., Feinberg, K., Carey, D.J., and Peles, E. (2007). Secreted gliomedin is a perinodal matrix component of peripheral nerves. J. Cell Biol. *177*, 551–562.

Eshed-Eisenbach, Y., and Peles, E. (2013). The making of a node: a co-production of neurons and glia. Curr. Opin. Neurobiol. *23*, 1049–1056.

Feinberg, K., Eshed-Eisenbach, Y., Frechter, S., Amor, V., Salomon, D., Sabanay, H., Dupree, J.L., Grumet, M., Brophy, P.J., Shrager, P., and Peles, E. (2010). A glial signal consisting of gliomedin and NrCAM clusters axonal Na+ channels during the formation of nodes of Ranvier. Neuron *65*, 490–502.

Ge, G., and Greenspan, D.S. (2006). Developmental roles of the BMP1/TLD metalloproteinases. Birth Defects Res. C Embryo Today *78*, 47–68.

Jaegle, M., Ghazvini, M., Mandemakers, W., Piirsoo, M., Driegen, S., Levavasseur, F., Raghoenath, S., Grosveld, F., and Meijer, D. (2003). The POU proteins Brn-2 and Oct-6 share important functions in Schwann cell development. Genes Dev. *17*, 1380–1391.

Labasque, M., Devaux, J.J., Lévêque, C., and Faivre-Sarrailh, C. (2011). Fibronectin type III-like domains of neurofascin-186 protein mediate gliomedin binding and its clustering at the developing nodes of Ranvier. J. Biol. Chem. *286*, 42426–42434.

Maertens, B., Hopkins, D., Franzke, C.W., Keene, D.R., Bruckner-Tuderman, L., Greenspan, D.S., and Koch, M. (2007). Cleavage and oligomerization of gliomedin, a transmembrane collagen required for node of ranvier formation. J. Biol. Chem. *282*, 10647–10659.

Maluenda, J., Manso, C., Quevarec, L., Vivanti, A., Marguet, F., Gonzales, M., Guimiot, F., Petit, F., Toutain, A., Whalen, S., et al. (2016). Mutations in GLDN, encoding gliomedin, a critical component of the nodes of Ranvier, are responsible for lethal arthrogryposis. Am. J. Hum. Genet. *99*, 928–933.

Muir, A.M., Ren, Y., Butz, D.H., Davis, N.A., Blank, R.D., Birk, D.E., Lee, S.J., Rowe, D., Feng, J.Q., and Greenspan, D.S. (2014). Induced ablation of Bmp1 and Tll1 produces osteogenesis imperfecta in mice. Hum. Mol. Genet. *23*, 3085–3101.

Peles, E., Nativ, M., Lustig, M., Grumet, M., Schilling, J., Martinez, R., Plowman, G.D., and Schlessinger, J. (1997). Identification of a novel contactin-associated transmembrane receptor with multiple domains implicated in protein-protein interactions. EMBO J. *16*, 978–988.

Rasband, M.N., and Peles, E. (2015). The nodes of Ranvier: molecular assembly and maintenance. Cold Spring Harb. Perspect. Biol. *8*, a020495.

Schafer, D.P., Custer, A.W., Shrager, P., and Rasband, M.N. (2006). Early events in node of Ranvier formation during myelination and remyelination in the PNS. Neuron Glia Biol. *2*, 69–79.

Schindelin, J., Arganda-Carreras, I., Frise, E., Kaynig, V., Longair, M., Pietzsch, T., Preibisch, S., Rueden, C., Saalfeld, S., Schmid, B., et al. (2012). Fiji: an open-source platform for biological-image analysis. Nat. Methods *9*, 676–682.

Talantikite, M., Lécorché, P., Beau, F., Damour, O., Becker-Pauly, C., Ho, W.B., Dive, V., Vadon-Le Goff, S., and Moali, C. (2018). Inhibitors of BMP-1/

Tolloid-like proteinases: efficacy, selectivity and cellular toxicity. FEBS Open Bio *8*, 2011–2021.

Vabnick, I., Novaković, S.D., Levinson, S.R., Schachner, M., and Shrager, P. (1996). The clustering of axonal sodium channels during development of the peripheral nervous system. J. Neurosci. *16*, 4914–4922.

Wambach, J.A., Stettner, G.M., Haack, T.B., Writzl, K., Škofljanec, A., Maver, A., Munell, F., Ossowski, S., Bosio, M., Wegner, D.J., et al. (2017). Survival among children with "lethal" congenital contracture syndrome 11 caused by novel mutations in the gliomedin gene (GLDN). Hum. Mutat. *38*, 1477–1484.

Zhang, Y., Bekku, Y., Dzhashiashvili, Y., Armenti, S., Meng, X., Sasaki, Y., Milbrandt, J., and Salzer, J.L. (2012). Assembly and maintenance of nodes of Ranvier rely on distinct sources of proteins and targeting mechanisms. Neuron *73*, 92–107.

STAR★METHODS

KEY RESOURCES TABLE

REAGENT or RESOURCE	SOURCE	IDENTIFIER
Antibodies		
Mouse anti-Myc	DSHB	AB_2266850
Mouse anti-MAG	EMD Millipore	AB_2137847
Rat anti-Neurofilament H	Millipore	Cat#MAB5448; PRID:AB_240852; PRID:AB_240852
Rabbit anti bIV Spectrin C9831	Dr. Matthew Rasband	N/A
Rabbit Caspr 6061	Peles et al., 1997	N/A
Chicken anti P0 F-1005	Aves Labs	CAT#F-1005
Mouse anti ankG	NeuroMab	clone N106/36
Mouse anti-Sodium Channel (PAN)	Sigma-Aldrich	clone K58/35; PRID:AB_477552
Rat anti MBP	Millipore	Cat#MAB386
Mouse anti gldn #94	Eshed et al., 2005	N/A
Rabbit anti gldn #386	Eshed et al., 2007	N/A
Chicken anti NFASC PAN	R&D systems	CAT#AF3235
Donky anti chicken 647	Jackson Laboratories	703-605-155
Donky anti chicken 488	Jackson Laboratories	703-545-155
Goat anti rabbit 488	Jackson Laboratories	111-545-144
Donky anti rabbit cy3	Jackson Laboratories	711-165-152
Donky anti mouse cy3	Jackson Laboratories	715-165-151
Donky anti mouse 647	Jackson Laboratories	715-605-140
Donky anti rat 647	Jackson Laboratories	712-605-153
Donky anti rat 405	Jackson Laboratories	712-475-153
Goat anti mouse IgG1	Jackson Laboratories	115-175-205
Bacterial and Virus strains		
XL10-Gold	Stratagene	Cat #200314
Chemicals, Peptides, and Recombinant Proteins		
Agar 100 Resin	Agar scientific	AGR1031
Uranyl Acetate 4%	Electron Microscopy Sciences	22400-4
Poly L-lysine	Sigma-Aldrich	Cat #P-1274
Trypsin (minus EDTA)	GIBCO	Cat #25050
B27-supplement	GIBCO	Cat #17504-044
FuDR	Sigma-Aldrich	Cat #F-0503
Glutamax	GIBCO	Cat# 15140-122
Mouse nerve growth factor (NGF)	Alomone labs	Cat# N-100
Sodium Pyruvate	GIBCO	Cat #11360039
Penicillin Streptomycin	GIBCO	Cat #15070063
DMEM-Medium	GIBCO	Cat #4196-039
Leibovitz l-15 medium	GIBCO	Cat# 11415064
Neurobasal medium	GIBCO	21103049
Basal medium Eagle	Sigma-Aldrich	B1522
ITS media supplement	Sigma-Aldrich	L3146
BSA	Sigma-Aldrich	A4503
D-Glucose	Sigma-Aldrich	G5146
Fetal Calf Serum	GIBCO	12657-029
Low IgG FCS	Thomas Scientific (Hyclone)	Cat#SH30898.02

(*Continued on next page*)

Continued

REAGENT or RESOURCE	SOURCE	IDENTIFIER
L-ascorbic acid	Sigma-Aldrich	A4544
Polybrene	Sigma-Aldrich	Cat#H9268
Forskolin	Sigma-Aldrich	Cat #F68886
Doxycycline	Sigma-Aldrich	Cat #D9891
PFA	Electron Microscopy Sciences	Cat# 15714
Cacodylate	Electron Microscopy Sciences	Cat# 11650
Glutaraldehyde	Electron Microscopy Sciences	Cat# 16220
Fluoromount-G	Thermo Fisher Scientific	Cat# 00-4958-02
Trypsin	GIBCO	Cat# 15090-046
Matrigel	Becton Dickinson	Cat#356234
Lipofectamine 2000	Thermo Fisher Scientific	Cat#11668030
Tri Reagent	Sigma-Aldrich	Cat#T9424
Proteinase inhibitor cocktail	MILIPORE	Cat# 539134-10ML
UK 383367	Santa Cruz Biochemistry	Cat#348622-88-8
Experimental Models: Cell Lines		
Phoenix-ECO	G. Nolan, Stanford, CA	N/A
Critical Commercial Assays		
Phusion High-Fidelity DNA Polymerase	NEB	M0530
KAPA HiFi HotStart Ready MixPCR Kit	KAPA BIOSYSTEMS	Cat# KK2600 07958919001
T4 DNA Ligase	Thermo Fisher Scientific	Cat# EL0014
Rneasy lipid tissue mini kit	QIAGEN	74804
SuperScriptII	Invitrogen	18064014
Experimental Models: Organisms/Strains		
Rat: Wistar	Envigo	N/A
Mouse: C57BL/6J	The Jackson Laboratory	Stock# 00064
Mouse: ICR (CD-1)	Envigo	N/A
mouse:Gliomedin KO	Feinberg et al., 2010	N/A
Mouse: BMP1/TLL1 double floxed	Muir et al., 2014	N/A
Mouse: Dhh-Cre	Jaegle et al., 2003	N/A
Recombinant DNA		
pMX-COL-myc	This paper	N/A
pMX-OLF-myc	This paper	N/A
pMX-ECD-myc	This paper	N/A
pMX-gldn-myc	This paper	N/A
pMX-dfurin-myc	This paper	N/A
pMX-dMBP-myc	This paper	N/A
TetOne-dfurin-myc	This paper	N/A
TetOne-Gldn-myc	This paper	N/A
pSx-FC	Eshed et al., 2007	N/A
pSx-ECD-FC	Eshed et al., 2007	N/A
Software and Algorithms		
FIJI	Schindelin et al., 2012	https://imagej.net/Fiji/Downloads
SerialEM	University of Colorado Boulder	https://bio3d.colorado.edu/SerialEM/
Ilastik	Berg et al., 2019	https://www.ilastik.org/
Qupath	Bankhead et al., 2017	https://qupath.github.io/
Zen 2012	Carl Zeiss	N/A
Adobe Photoshop CC 2019	Adobe	N/A

(*Continued on next page*)

Continued

REAGENT or RESOURCE	SOURCE	IDENTIFIER
pCLAMP 10.2	Molecular Devices, Sunnyvale, CA	N/A
Clampfit 10.2	Molecular Devices	N/A
Deposited Data		
G ration macro/PNS (Fiji)	This paper	https://github.com/WIS-MICC-CellObservatory/Myein_Profiles_PNS
Other		
LSM700 confocal microscope	Carl Zeiss	N/A
Pannoramic digital slide scanner	3DHISTECH	N/A
Philips CM-12 transmission electron microscope	FEI	N/A
Axioskop 2 microscope with Apotom	Carl Zeiss	N/A
Primaria cell culture dish	Corning (Falcon)	Cat#353803
Poly-Prep Chromatography Columns	Bio-Rad	Cat#7311550
Homogenizing pestles in G-tubes	Thomas Scientific	1212M63

LEAD CONTACT AND MATERIALS AVAILABILITY

Further information and requests for resources and reagents should be directed to and will be fulfilled by the Lead Contact, Elior Peles (peles@weizmann.ac.il). All unique/stable reagents generated in this study are available from the Lead Contact with a completed Materials Transfer Agreement.

EXPERIMENTAL MODEL AND SUBJECT DETAILS

Mouse Models

Mouse embryos at postnatal day P0-5 and adult mice at P75 were used in this study as indicated. Mice were kept on ICR (CD-1) background. Gliomedin null (Feinberg et al., 2010) and BMP1/TLL1 double floxed (Muir et al., 2014) mice were previously described. Double floxed mice were crossed with mice carrying a transgenic cre under the control of the DHH promoter, expressed specifically in myelinating Schwann cells (SCs) (Jaegle et al., 2003). Genotyping was carried out by PCR on genomic DNA extracted from mouse tails. For sciatic nerve crush experiments, female C57BL/6J were used. For all experiments, both male and female littermates were randomly assigned to experimental groups. Animals were housed in a temperature-controlled animal room with a 12 hours light/dark cycle. Water and food were available *ad libitum*. All experiments were performed in compliance with the relevant laws and institutional guidelines and were approved by the Weizmann Institute's Animal Care and Use Committee.

Primary Cultures

Dissociated DRG cultures were prepared from mouse embryos at day 13.5 of gestation. Embryos' tails were used for genotyping. DRGs collected from embryos of matching genotypes were pulled, dissociated and plated at a density of 4×10^4 per 13 mm slide, coated with Matrigel and Poly-L-lysine. Cultures were grown for 2 days in Neurobasal medium supplemented with B-27, glutamax, penicillin /streptomycin and 50 ng/ml NGF. Cultures were then grown for 4-5 additional days in BN medium containing Basal medium-Eagle, ITS supplement, glutamax, 0.2% BSA, 4 mg/ml D-glucose, 50 ng/ml NGF and antibiotics. To induce myelination, cultures were grown in BNC, namely a BN medium supplemented with 15% heat inactivated fetal calf serum (replacing the BSA) and 50 μg/ml L- ascorbic acid. Cultures were fixed after 10 additional days. For retroviral infection, cultures were incubated with retrovirus-containing media supplemented with 5 μg/ml Polybrene for 3 hours, for three consecutive days, starting one day after plating.

In the case of Tetracycline-inducible viruses, myelinating media was supplemented with doxycycline at 1 μg/ml. For FC-fusion proteins addition, FC proteins were added to the BNC media. Rat Schwann cell cultures were prepared from confluent DRG cultures that had been trypsinized and allowed to adhere to Primaria culture dishes at 37°C for 30 (first passage) to 10 minutes (last passage). Plates were washed of un-adhered cells and kept in rat Schwann cell medium (DMEM, 3% FBS, 10% NDFβ conditioned medium, 2 μM forskolin, 2 mM glutamax, and 1 mM pyruvate) until confluent. Cultures were similarly passaged until purity (i.e., fibroblast-free). Transfection of SCs was done using the Lipofectamine 2000 reagent. To stimulate ECM assembly, Schwann cells were treated with 50 μg/ml L-ascorbic acid for 48 to 72 hours. To remove cells from the culture dish in order to label the remaining ECM, cultures were treated with PBS + 0.5% Triton X-100 and 20 mM ammonium hydroxide for 10 s and subsequently washed with PBS.

METHOD DETAILS

Generation of gliomedin expression and viral plasmids

Retroviral plasmids pMX-COL-myc, pMX-OLF-myc, and pMX-ECD-myc were generated by cloning PCR fragments of the following sequences from the gliomedin ORF: COL (residues 49–294), OLF (residues 288–543), ECD (residues 49–543), into retroviral vector pMX. Myc tag was added at the C terminus. The mutant gliomedin dBMP construct (two amino acid substitutions DD278AA) was generated using pcDNA3-gldn as template by PCR using 5′ primer gtgtgtcatacccaatgctgcaaccttggtggggagag and its complementary 3′ primer. Primers used for the generation of the dfurin (R91G,R94A) mutations were previously described (Eshed et al., 2007). Mutant and WT gliomedin ORF sequences were subsequently sub-cloned into pMX. In order to generate viruses carrying Tet-inducible gliomedin constructs, we constructed a pMX-based vector that contained the tet-on 3G transactivator and the Tres3G promoter from a pLVX - TetOne vector (Clontech). WT and dBMP gliomedin ORFs were sub-cloned into this vector (pMX-tetOne).

Production of retroviruses

For retroviral stock preparation, helper virus-free Phoenix-Eco packaging cells were transfected by the $CaPO_4$ method with the various pMX-gliomedin-myc constructs. Medium was changed a day after transfection and collected after additional 24 hours. Virus-containing media were centrifuged at 1500 RPM for 5 minutes to remove cells and stored at −80°C until use.

Fc-fusion protein production and purification

HEK293T cells were transfected by the $CaPO_4$ method with pSx-FC and pSx-ECD-FC constructs. Medium was changed to DMEM+2% low IgG FCS a day after transfection and collected after an additional 48-72 hours. Conditioned media were filtered to remove cells and stored at 4°C until use. For protein purification, media were incubated with protein A-coupled agarose for 2 hours at RT. After extensive washes with PBS in chromatography columns, proteins were eluted by glycine 0.1 M, pH2.5 into tubes containing 1 M Tris in an adjusted volume for titration to pH7.

Reverse transcription PCR

Total RNA was isolated from brain and cell cultures using Tri Reagent, and from Sciatic nerve using RNeasy lipid tissue kit. cDNA was synthesized by SuperScript II using an oligo dT primer.

Immunofluorescent labeling

For immunofluorescent labeling of cell culture samples, cultures were fixed with 4% PFA for 10 minutes at RT. Sciatic nerves isolated from mouse pups were fixed in 4% PFA for 5 (P0) to 8 (P5) minutes at RT and kept at 20% sucrose/PBS until used for teasing or cryosectioning (using Leica CM1950) of the entire sciatic nerve or the common peroneal nerve branch alone. Samples were incubated in blocking solution (PBS, 1% glycine, 5% normal goat serum, 0.5% Triton X-100) for 45 minutes at RT and were subsequently incubated over-night at 4°C with primary antibodies, diluted in blocking solution containing 0.1% Triton X-100. After extensive washing with PBS, samples were incubated with fluorophore-conjugated secondary antibodies for 45 minutes at RT, and were next washed and mounted in Fluoromount-G. For staining whole mount nerve samples, fixed nerves were incubated in PBS with 2% Triton X-100 for 30 minutes while shaking, followed by 30 minutes in blocking buffer containing PBS+1% Triton X-100 and 4% BSA. Samples were then incubated ON at 4°C while shaking with primary antibodies diluted in blocking buffer. The next day, samples were extensively washed in PBS and incubated with secondary antibodies in blocking buffer while shaking for 2 hours at RT. Samples were lastly washed and mounted. Fluorescence images were obtained using an Axioskop 2 microscope equipped with an Apotome imaging system (Carl Zeiss), fitted with a Hamamatsu ORCA-ER CCD camera, or using an LSM700 confocal microscope (Carl Zeiss). For large-area imaging of DRG cultures a slide scanner (Panoramic Midi Digital Scanner, 3DHISTECH) was used. Whole slide images were exported as TIFF files via Qupath software and analyzed using FIJI. For experiments involving mouse tissues, at least three mice were used per genotype, and at least three images from each mouse was used for quantitative image analysis. Experiments that involved tissue culture systems were repeated at least three times, and at least three images for every condition were used for image analysis . Tissue culture samples were numbered randomly and quantitated blindly.

Immunoprecipitation and immunoblot analysis

For immunoprecipitation, DRG cultures conditioned media were immunoprecipitated by polyclonal rabbit anti-gliomedin antibodies #386 bound to protein A–agarose beads. For analysis of cell lystates, cultures were lysed in 50 mM HEPES, pH 7.2, 150 mM NaCl, 1 mM EGTA, 10% glycerol, 1% Triton X-100, 2 mM PMSF, with protease inhibitor cocktail. Samples were subsequently analyzed by electrophoresis on 10% polyacrylamide SDS gels and immunoblotted using anti-myc antibodies. Sciatic nerves were lysed in laemmli sample buffer using dounce homogenizer (adult nerve) or microcentrifuge tube-fitted homogenizing pestle (P3 and P6).

Electrophysiology

Recordings were performed at P2, P3, P5, P12 and P50. Each age included at least 3 (maximum of 5) mice per genotype, both sciatic nerves were analyzed for each mouse . After euthanasia, sciatic nerves were quickly dissected and transferred into artificial cerebrospinal fluid (aCSF) equilibrated with 95% O_2-5% CO_2, which contained (in mM) 126 NaCl, 3 KCl, 2 $CaCl_2$, 2 $MgSO_4$, 1.25

NaH_2PO_4, 26 $NaHCO_3$, and 10 dextrose, pH 7.4-7.5. Recordings of P2 to P12 nerves were performed using two suction glass electrodes filled with aCSF. Compound action potentials (CAPs) were evoked by applying a supramaximal stimulus (40 μs duration) from one electrode and were recorded from the second electrode. For P50 animals, sciatic nerves were cut into 2 cm segments and placed into a three-compartment recording chamber. The distal end was stimulated supramaximally (40 μs duration) through two electrodes isolated with Vaseline, and recordings were performed at the proximal end. In both experiments, nerves were continuously perfused (1-2 ml/min) with 35°C oxygenated aCSF. Signals were amplified, digitized at 500 kHz, and acquired using pCLAMP 10.2 software (Molecular Devices, Sunnyvale, CA). Conduction velocities (CV) were estimated from latencies. The delays of the CAPs were calculated at half the maximal amplitude ($V_{1/2}$) and at the maximal amplitude (Vmax). The duration of the CAPs was calculated at half the maximal amplitude. When multiphasic components were recorded (at P2 and P3), the delay of the fastest and slowest peaks were measured (CV fast and CV slow). For recruitment analysis, nerves were stimulated at increasing intensities. For refractory period analysis, two stimuli were applied at different intervals, and the amplitude of the second CAP was measured and plotted as a function of the stimulus interval. At P2 and P3, a Gaussian function was fit to the data using Clampfit 10.2 (Molecular Devices).

Sciatic nerve crush

Seven to 11 weeks old female mice (C57BL/6J) were used. All procedures were approved by the Institutional Animal Care and Use Committee at Baylor College of Medicine, and conform to the United States Public Health Service Policy on Human Care and Use of Laboratory Animals. Mice were anesthetized by isoflurane. The left sciatic nerve was exposed and crushed for 10 s periods at the level of the sciatic notch using forceps (No. 5). Seven- and nine-days post crush (dpc), 2 μl of UK383367 solution (1 μM), or vehicle (0.001% DMSO in Locke's solution) was injected into tibial nerves 4 mm distal to the crush sites. At 12 dpc, the tibial nerves were rapidly dissected out after killing mice by inhalation of isoflurane. The tissues were fixed in 4% paraformaldehyde in 0.1 M PB for 30 min, immersed into 20% sucrose in 0.1M PB at 4°C overnight, and then embedded in OCT compound. Sections of 16 μm were cut by cryostat and mounted on gelatin-coated coverslips.

Image Processing and Analysis

For fluorescence images, processing included only global change of contrast and brightness. For image analysis, images were taken in equivalent spatial distribution. Figures display representative images. Image analysis was performed using ImageJ (NIH) and ZEN 2011 (Carl Zeiss) software.

Electron Microscopy

Mice were scarified and sciatic nerves were exposed and fixed with 4% PFA, 2.5% glutaraldehyde in 0.1M cacodylate buffer (pH 7.4). Nerves were then excised and incubated over-night in the same fixative at room temperature and stored at 4°C. Nerves were processed as previously described (Feinberg et al., 2010), and were examined using a FEI Tecnai Spirit transmission electron microscope coupled with an FEI Eagle camera. For G ratio analysis samples were examined using a FEI Tecnai T12 transmission electron microscope or Tecnai F20 S/TEM equipped with a XF416 TVIP camera or a US4000 Gatan camera, respectively. SerialEM software was used for montage assembly allowing high resolution imaging of the entire nerve cross section. At least 250 axon per mouse were measured.

Intact myelin profiles were counted and quantified using the following protocol: Ilastik (Berg et al., 2019) pixel classifier was trained to classify pixels into myelin/background on selected small parts of the images. A dedicated Fiji (Schindelin et al., 2012) macro (available at https://github.com/WIS-MICC-CellObservatory/Myein_Profiles_PNS) applied this classifier to each image and created a binary mask of candidate myelin pixels. Candidate myelin segments were extracted using connected component analysis and further filtered based on myelin-segment size (> 3.8 um^2), inner –hole area (> 7.6 um^2), inner hole circularity (> 0.1), and area fraction (< 90%) to make sure that only closed profiles are taken into account. Twisted profiles were discarded by filtering out segments with more than one hole. Inner and outer contours were extracted from each segment and used for calculating the inner and outer area. G-ratio was then calculated for each profile as the ratio between the equivalent inner and outer diameters. This automatic process segmented correctly most of the profiles. Further manual correction was done to add non-detected profiles, delete falsely detected objects and fix for segmentation errors. All the measurements were recalculated based on the corrected segments. The macro allows for this by saving matched pairs of inner and outer contours in a file, and by providing update mode to calculate the measurements from a segments file. The number of profiles in each image was normalized by the size of the tissue which was extracted manually. Analysis was done after downscaling the images by factor of 2, to allow for feasible processing time.

QUANTIFICATION AND STATISTICAL ANALYSIS

Statistical tests were done using Microsoft Excel, n represents the number of independent tissue culture experiments or the number of mice of the same genotype or experimental group. For experiments in which multiple samples were compared (Figures 1C, 1D, and 2B), statistical significance was determined using two-tailed t test according to the Bonferroni correction. For the analyses of tissue culture-based experiments we used three independent cultures each. Fields of view were randomly chosen and cluster numbers were determined by FIJI. Analysis of nodal-like cluster density in the developing sciatic nerve (Figure 4B) was done by normalizing cluster density with total DAPI-occupied area, as calculated by FIJI. At least 4 mice were included in each experimental

group at each postnatal day. For the analysis of Caspr staining adjacent to nodal-like clusters in the developing sciatic nerve (Figure 4D), cluster detection was done by FIJI, whereas the adjacent Caspr labeling was counted manually, with at least three mice in each group for each of the postnatal days tested.

DATA AND CODE AVAILABILITY

This study did not generate any unique datasets. A Fiji macro that was used in Figure S4 is available at https://github.com/WIS-MICC-CellObservatory/Myein_Profiles_PNS.

Neuron, Volume *106*

Supplemental Information

Precise Spatiotemporal Control of Nodal Na^+ Channel Clustering by Bone Morphogenetic Protein-1/Tolloid-like Proteinases

Yael Eshed-Eisenbach, Jerome Devaux, Anna Vainshtein, Ofra Golani, Se-Jin Lee, Konstantin Feinberg, Natasha Sukhanov, Daniel S. Greenspan, Keiichiro Susuki, Matthew N. Rasband, and Elior Peles

SUPPLEMENTARY FIGURES

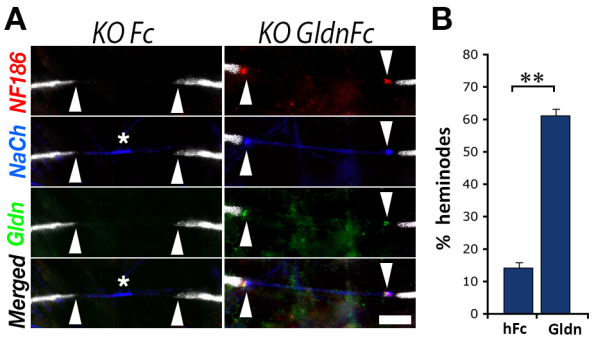

Supplementary Figure 1. Soluble gliomedin rescues heminodal clustering in *Gldn*$^{-/-}$ DRG culture. (*Related to Figure 1*).
A. Myelinated Schwann cells/DRG neuron cultures prepared from *gldn*$^{-/-}$ mice were grown in the presence of soluble gliomedin fused to human Fc (*KO GldnFc*) or human Fc as control (*KO Fc*). Immunolabeling was carried out using antibodies to NF186, Na^+ channels (NaCh), gliomedin (Gldn) and MBP. MBP immunoreactivity (white) is shown in all panels. Gldn-Fc bound to heminodes (arrowheads), where it induced clustering of NF186 and Na^+ channels. Binding of Gldn-Fc is also noted throughout the slide to extracellular material deposited by Schwann cells. An asterisk marks the abnormal accumulation of Na^+ channels along the gap between two myelin segments in the absence of gliomedin. **B**. Quantification of the results showing the percentage of myelinated axonal segments associated with heminodal clusters of Na^+ channels in each of these cultures (**P<0.005; *n*=3 different primary cultures, total of 100 MBP-positive segments counted). Scale bars, A, C, 15 µm.

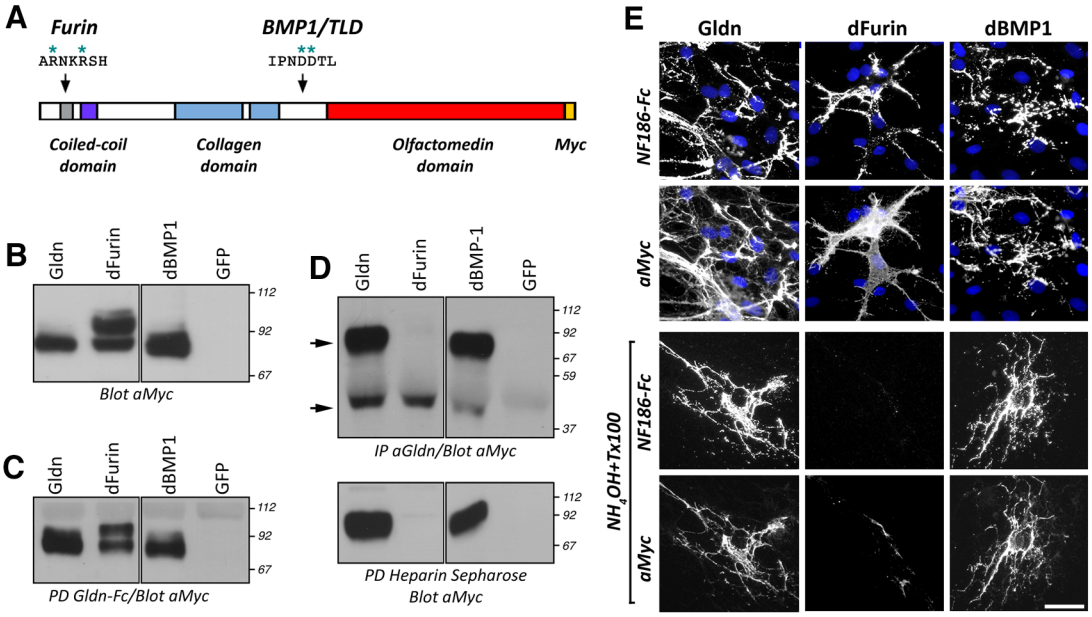

Supplementary Figure 2. Characterization of two protease-resistant gliomedin mutant proteins. (*Related to Figure 1 and Figure 2*).

A. Domain organization of gliomedin. **B**. Western blot analysis of cell lysates of HEK-293T cells expressing myc-tagged versions of full-length wild type gliomedin (Gldn), or protease-resistant mutants of gliomedin lacking the furin (dFurin) or BMP1/TLD (dBMP1) cleavage sites, using an antibody to myc-tag. The locations of molecular mass markers are shown on the right in kDa. **C**. Gliomedin mutants retain their ability to self-associate. The indicated cell lysates were incubated with the extracellular domain of gliomedin (Gldn-Fc) immobilized to protein A beads. Pulled-down proteins were separated in an SDS-PAGE gel and immunoblotted with an antibody to myc-tag. **D**. Conditioned media collected from the same cultures were subjected to immunoprecipitation using an antibody to gliomedin (upper panel), or to pull-down with heparin-Sepharose beads (lower panel). Protein complexes were separated on SDS-PAGE and subjected to Western blot analysis using an antibody to myc-Tag. Note that the dFurin gliomedin mutant is not detected in the medium. **E**. Gliomedin mutants retain their ability to bind NF186. Schwann cells transfected with a full-length, or the two protease-resistant gliomedin mutants, were treated with ascorbic acid for 48 hours before they were allowed to bind to a soluble fusion protein containing the extracellular domain of NF186 (NF186-Fc). The cultures were then fixed and immunolabeled with an antibody to Myc-tag (αMyc). The lower panels show a similar experiment in which the slides were treated with ammonium hydroxide and triton X-100 to remove the cells before fixation and immunolabeling. Note that dBMP1, but not dFurin mutant was incorporated into the Schwann cell ECM, similar to full-length gliomedin. Scale bars, 30 μm.

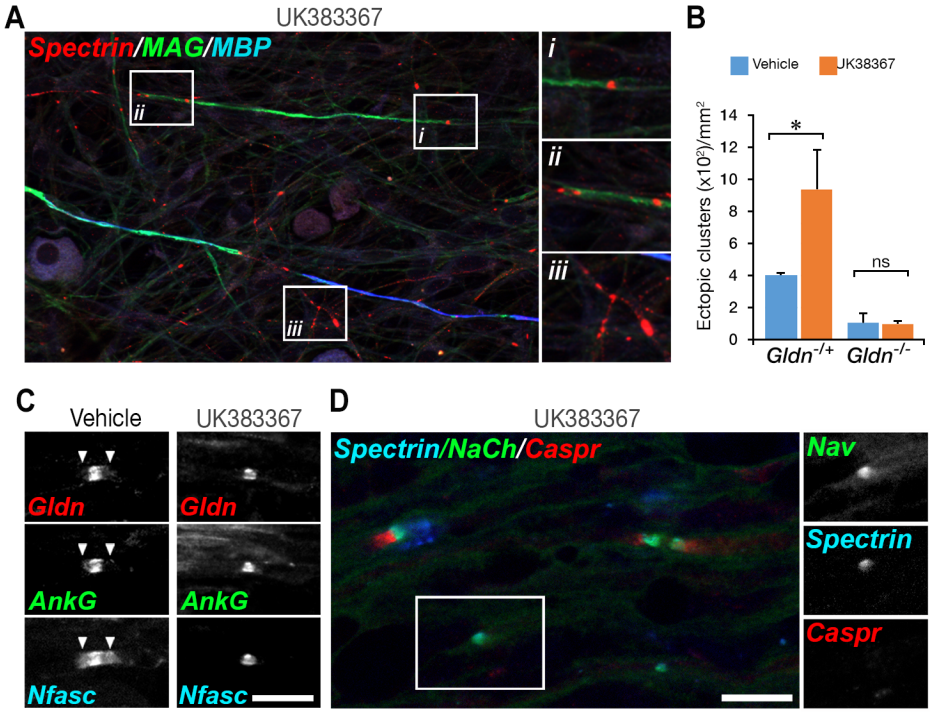

Supplementary Figure 3. Pharmacological inhibition of BMP-1/tolloid-like proteinases enhances the sodium channel clustering activity of gliomedin. (*Related to Figure 2*).
A. Representative image of UK383367-treated Schwann cell/DRG neuron cultures immunolabeled for βIV spectrin (Spectrin), MAG, and MBP. Note the presence of nodal clusters at heminode flanking MAG positive but MBP negative internodes (*i* and *ii*), below the forming internode (iii) and at ectopic sites not associated with differentiating Schwann cells (*iii*). Insets show higher magnification of the boxed areas. **B.** Induction of ectopic clusters by UK383367 requires gliomedin. Quantification of the number of ectopic clusters per square millimeter (mm^2) detected in myelinated Schwann cell/DRG neuron cultures that were prepared from gliomedin null (*gldn*$^{-/-}$) and heterozygous control (*gldn*$^{-/+}$) mice. Cultures were left untreated (Vehicles) or grown in the presence of UK383367 (n=3; *$p < 0.02$). **C.** Longitudinal section of tibial nerve at 12 days post crush immunolabeled using antibodies to neurofascin (Nfasc), ankyrin G (AnkG), and gliomedin (Gldn). Vehicle control or BMP1 inhibitor (UK383367) was injected at seven and nine dpc. Representative images of mature node (Vehicle) or immature node without associated paranodes (UK383367) are shown. Anti-Nfasc antibody labels nodal NF186 strongly (colocalizing with gliomedin and ankyrin G immunoreactivity) and paranodal NF155 weakly (arrowheads, left column). **D.** Longitudinal section of tibial nerve at 12 days post crush immunolabeled using antibodies to βIV spectrin (Spectrin), Na^+ channels (NaCh), and Caspr showing the presence of clusters with no associated Caspr immunostaining (box). Individual color images of boxed area are shown in the right column. Scale bars, A, 50 μm, D-E, 10 μm.

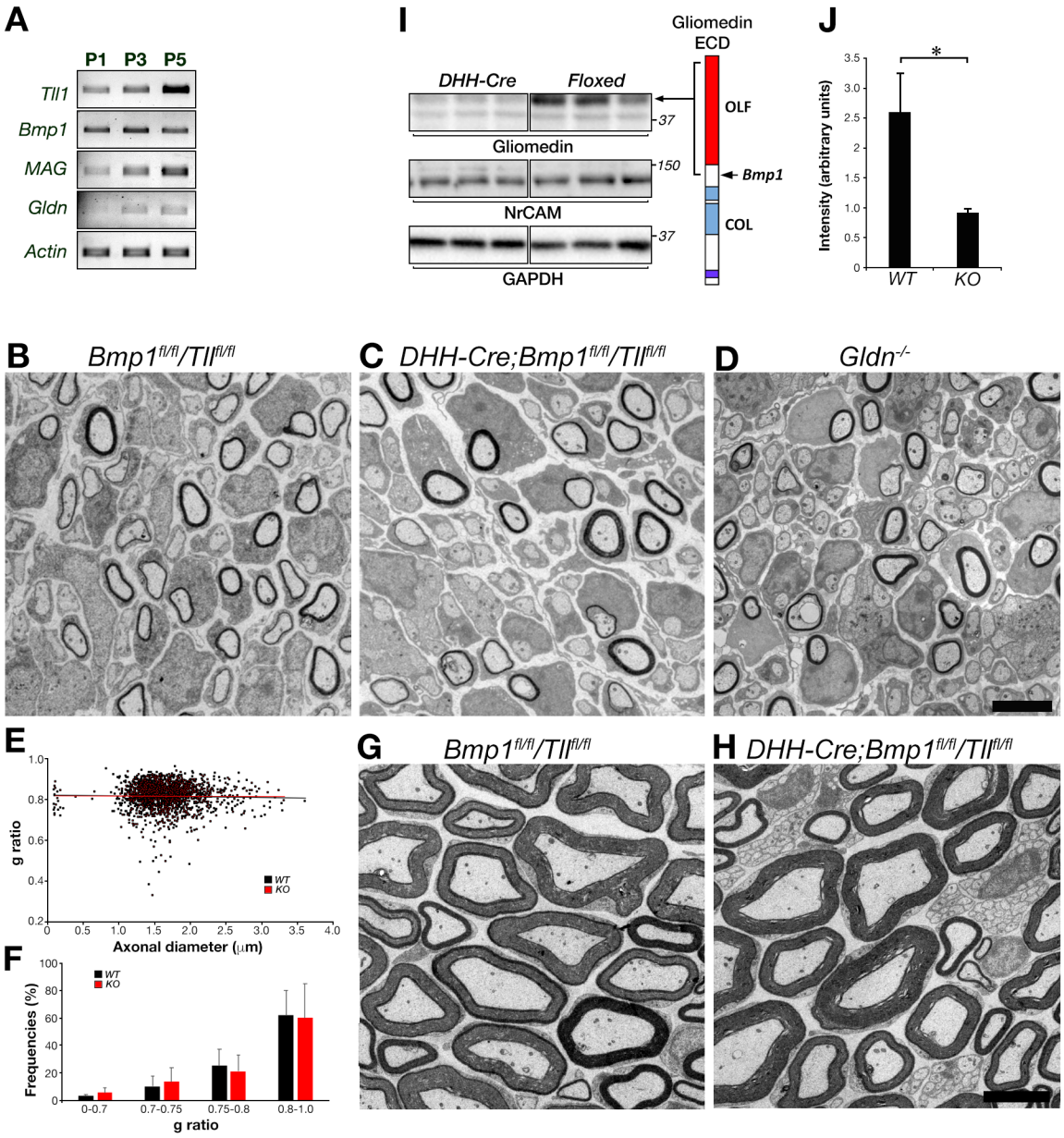

Supplementary Figure 4. Characterization of mice lacking both *Bmp1* and *Tll1* in Schwann cells. (*Related to Figure 3*).

A. RT-PCR analysis of sciatic nerve isolated from P1-P5 wild type mice using primers specific toTll1, Bmp1, MAG, Gliomedin (Gldn) and actin as indicated. **B-D.** Representative electron microscopy images of sciatic nerve sections obtained from P3 control mice carrying floxed alleles of *Bmp1* and *Tll1* (B, $Bmp1^{fl/fl}/Tll^{fl/fl}$), animals in which these genes were deleted in Schwann cells using DHH-Cre (C, $DHH\text{-}Cre;Bmp1^{fl/fl}/Tll^{fl/fl}$), or Gliomedin null (D, $Gldn^{-/-}$) mice as indicated. **E.** g-ratio of $Bmp1^{fl/fl}/Tll^{fl/fl}$ (*WT*) and $DHH\text{-}Cre;Bmp1^{fl/fl}/Tll^{fl/fl}$ (*KO*) as a function of axonal diameter. Total of at least 750 axons from 3 mice of each genotype were analyzed. The average g ratio at p3 was 0.81±0.06 for both $Bmp1^{fl/fl}/Tll^{fl/fl}$ and $DHH\text{-}Cre;Bmp1^{fl/fl}/Tll^{fl/fl}$, and 0.80±0.04 for $Gldn^{-/-}$ mice. **F.** Frequency distribution of myelinated axons according to their diameters. **G-H.** Electron microscopy images of sciatic nerve cross sections obtained from P30 $Bmp1^{fl/fl}/Tll^{fl/fl}$ (*WT*) or $DHH\text{-}Cre;Bmp1^{fl/fl}/Tll^{fl/fl}$ (*KO*) mice, revealing the presence of normal myelinated axons in both genotypes. **I.** Western blot analysis of sciatic nerves isolated $DHH\text{-}Cre;Bmp1^{fl/fl}/Tll^{fl/fl}$ and control $Bmp1^{fl/fl}/Tll^{fl/fl}$ mice at P3 using antibodies to gliomedin and GAPDH as indicated. **J.** Quantification of the results shown in panel I. Values are normalized to GAPDH. *WT,* $Bmp1^{fl/fl}/Tll^{fl/fl}$; *KO,* $DHH\text{-}Cre;Bmp1^{fl/fl}/Tll^{fl/fl}$ (*n*=3; *p<0.03, Student's t test). Scale bars, B-D, 2 μm, G-H, 5 μm. **SUPPLEMENTARY TABLES**

		Amplitude	Duration	Conduction velocities ($m.s^{-1}$)				
		(mV)	$V_{1/2}$ (ms)	Vmax	$V_{1/2}$	Fast peak	Slow peak	*n*
P2	Control	0.50 ± 0.31	2.7 ± 0.5	1.4 ± 0.1	2.4 ± 0.3	N.A.	N.A.	6
	dKO	0.25 ± 0.14	2.6 ± 1.2	1.9 ± 0.7	2.8 ± 0.9	2.5 ± 0.4‡	1.4 ± 0.4	8
P3	Control	0.21 ± 0.1	4.9 ± 1.2	2.1 ± 0.9	3.5 ± 0.7	2.9 ± 0.6	0.9 ± 0.2	9
	dKO	0.28 ± 0.12	3.6 ± 2.0	2.9 ± 1.3	4.5 ± 0.9*	3.7 ± 0.6*	0.9 ± 0.2	8
P5	Control	0.41 ± 0.12	1.1 ± 0.2	5.4 ± 1.2	7.3 ± 1.4			6
	dKO	0.29 ± 0.07	1.1 ± 0.3	5.9 ± 1.0	7.9 ± 1.4			8
P50	Control	3.36 ± 1.53	0.9 ± 0.5	42.6 ± 4.6	63.2 ± 6.3			8
	dKO	4.91 ±2.10	0.8 ± 0.4	44.0 ± 5.9	66.1 ± 8.2			10

Supplementary Table 1. Characteristics of CAPs from neonatal sciatic nerves of *DHH-Cre;Bmp1$^{fl/fl}$/Tll$^{fl/fl}$* (dKO) and *Bmp1$^{fl/fl}$/Tll$^{fl/fl}$* (Control) mice (*Related to Figure 3*). Data are represented as mean ± S.D. ‡ Significantly different from control Vmax value P<0.01 with a two-tailed t-tests for two samples of equal variance; * Significantly different from control values P<0.01 with a two-tailed t-tests for two samples of equal variance. n represents the number of nerves tested. N.A. = not applicable; Vmax = at maximal peak amplitude; $V_{1/2}$ = at half the maximal amplitude.